Nuclear Medicine and Biology 43 (2016) 415–423

Contents lists available at ScienceDirect

Nuclear Medicine and Biology

journal homepage: www.elsevier.com/locate/nucmedbio

Research paper

Biodistribution of ^{125}I-labeled anti-endoglin antibody using SPECT/CT imaging: Impact of *in vivo* deiodination on tumor accumulation in mice

Linda Karmani [a], Philippe Levêque [a], Caroline Bouzin [b], Anne Bol [c], Marc Dieu [d], Stephan Walrand [c], Thierry Vander Borght [c], Olivier Feron [b], Vincent Grégoire [c], Davide Bonifazi [e], Carine Michiels [d], Stéphane Lucas [f], Bernard Gallez [a,*]

[a] Biomedical Magnetic Resonance Research Group (REMA), Louvain Drug Research Institute (LDRI), Université Catholique de Louvain, Avenue Mounier 73, 1200, Brussels, Belgium
[b] Pharmacology and Therapeutics Unit (FATH), Institute of Experimental and Clinical Research (IREC), Université Catholique de Louvain, Avenue Mounier 53, 1200, Brussels, Belgium
[c] Centre for Molecular Imaging, Radiotherapy and Oncology (MIRO), Institute of Experimental and Clinical Research (IREC), Université Catholique de Louvain, Avenue Hippocrate 54, 1200, Brussels, Belgium
[d] Unité de Recherche en Biologie Cellulaire (URBC), Namur Research Institute for Life Sciences (NARILIS), University of Namur, Rue de Bruxelles 61, 5000, Namur, Belgium
[e] Namur Research College and Department of Chemistry (NARC), University of Namur, Rue de Bruxelles 61, 5000, Namur, Belgium
[f] Research Centre for the Physics of Matter and Radiation (PMR), Namur Research Institute for Life Sciences (NARILIS), University of Namur, Rue de Bruxelles 61, 5000, Namur, Belgium

ARTICLE INFO

Article history:
Received 14 March 2016
Received in revised form 25 March 2016
Accepted 26 March 2016
Available online xxxx

Keywords:
Anti-endoglin antibody
Deiodination
CD105
Tumor
KRYRR
SPECT/CT

ABSTRACT

Introduction: Radiolabeled antibodies directed against endoglin (CD105) are promising tools for imaging and antiangiogenic cancer therapy. To validate iodinated antibodies as reliable tracers, we investigated the influence of the radiolabeling method (direct or indirect) on their *in vivo* stability.
Methods: Anti-CD105 mAbs were radioiodinated directly using chloramine-T (^{125}I-anti-CD105-mAbs) or indirectly using D-KRYRR peptide as a linker (^{125}I-KRYRR-anti-CD105-mAbs). The biodistribution was studied in B16 tumor-bearing mice *via* SPECT/CT imaging.
Results: Radioiodinated mAbs were stable *in vitro*. *In vivo*, thyroid showed the most important increase of uptake after 24 h for ^{125}I-anti-CD105-mAbs (91.9 ± 4.0%ID/ml) *versus* ^{125}I-KRYRR-anti-CD105-mAbs (4.4 ± 0.6%ID/ml). Tumor uptake of ^{125}I-anti-CD105-mAbs (0.9 ± 0.3%ID/ml) was significantly lower than that of ^{125}I-KRYRR-anti-CD105-mAbs (4.7 ± 0.2%ID/ml).
Conclusions: An accurate characterization of the *in vivo* stability of radioiodinated mAbs and the choice of an appropriate method for the radioiodination are required, especially for novel targets. The indirect radioiodination of internalizing anti-CD105 mAbs leads to more stable tracer by decreasing *in vivo* deiodination and improves the tumor retention of radioiodinated mAbs.
Advances in knowledge and implications for patient care: To date, the only antiangiogenic antibody approved for clinical indications is bevacizumab. There is a need to develop more antibodies that have targets highly expressed on tumor endothelium. CD105 represents a promising marker of angiogenesis, but its therapeutic relevance in cancer needs to be further investigated. In this context, this study suggests the potential use of indirectly iodinated anti-CD105 mAbs for tumor imaging and for therapeutic purposes.

1. Introduction

Endoglin (CD105) is an auxiliary receptor for transforming growth factor-β (TGF-β) [1]. CD105 is expressed on vascular endothelial cells and overexpressed in proliferating endothelial cells of tissues undergoing angiogenesis, such as regenerated and inflamed tissues or tumors [2–4]. CD105 is highly expressed in tumor-associated endothelium in many solid cancers, including breast, prostate and cervical cancer [2,5–7]. CD105 may also be abundantly expressed in some cancer cells, such as melanoma [8,9] and choriocarcinoma cells [10]. Several studies have indicated that CD105 represents a more specific and sensitive marker for tumor angiogenesis and tumor progression than the commonly used pan-endothelial markers, such as CD34 and CD31 [11,12]. Indeed, the vascular density, determined by using anti-CD105 antibodies, was correlated with the prognosis of breast cancer patients [13], with the risk of developing metastatic disease in colorectal cancer [14], and with the recurrence of malignancy of head and neck squamous cell carcinoma [15]. Clinical trials are currently in progress and their results may validate CD105 as a novel target for cancer treatment [16].

Non-invasive molecular imaging of malignancies using radiolabeled anti-CD105 mAbs as specific tracers is an attractive strategy that can

* Corresponding author at: Biomedical Magnetic Resonance Research Group, Louvain Drug Research Institute, Université Catholique de Louvain, Avenue Mounier 73 - B1.73.08, B-1200, Brussels, Belgium. Tel.: +32 2 7647391; fax: +32 2 7647390.
E-mail address: Bernard.Gallez@uclouvain.be (B. Gallez).

http://dx.doi.org/10.1016/j.nucmedbio.2016.03.007
0969-8051/

improve cancer detection, tumor characterization, and therapy efficiency [17]. For a long time, the radionuclides of iodine have been widely used to radiolabel mAbs, peptides and other biomolecules because they are readily available, at reasonable costs, with simple radiolabeling procedures. These radioiodinated tracers were largely used to study tumor targeting for cancer imaging (^{123}I, ^{124}I, ^{125}I), for cancer therapy (^{131}I), and for an approach in which imaging is performed as a scouting procedure before radioimmunotherapy to confirm tumor targeting and to assess tissue dosimetry [18].

Many different strategies are available for radioiodination of proteins. Generally, radioiodination procedure consists in direct oxidation of iodine to label tyrosine residues of proteins. In most cases, the biological distribution studies do not assess the effect of *in vivo* deiodination on tumor targeting [3,19–23]. Moreover, specifically for anti-endoglin antibodies, some studies have continued to describe the biological distribution and the tumor targeting by using directly radioiodinated anti-CD105 mAbs, without assessing the extent of *in vivo* deiodination and its influence on the radioactivity uptake in tissues [3,19]. However, the role of metabolism after the antibody internalization in tumor cells and the subsequent fate of the attached radionuclide are issues that need to be considered because these processes affect the tumor accumulation [24,25]. Indeed, the antibody dehalogenation was observed using mAbs obtained by direct radioiodination method [20,26–29]. To overcome this problem, strategies that use indirect radiohalogenation reactions have been developed to improve the *in vivo* stability and to decrease the nonspecific tissue uptake, while retaining the tumor uptake and preserving a satisfactory tumor contrast [24,30–35].

In the present study, anti-CD105 mAbs were radiolabeled using two methods, either direct radioiodination with chloramine-T as oxidizing agent, or indirect radioiodination with a bifunctional reagent as a linker between the iodine and the antibody. The chosen linker was a peptide prosthetic group, assembled with five D-amino acids, including D-tyrosine (D-Lys-Arg-Tyr-Arg-Arg, D-KRYRR). *D-KRYRR is positively charged at lysosomal pH and should be trapped in lysosomes after the antibody internalization into cells* [26]. *In vitro* stability of ^{125}I-labeled anti-CD105 mAbs was investigated as well as *in vivo* the distribution of radioiodinated mAbs through SPECT/CT imaging. We compared the biodistribution profile of directly and indirectly radiohalogenated mAbs in order to explore the impact of the radioiodination method on the tumor uptake of the tracer, the nonspecific tissue accumulation, and the imaging properties. Finally, the tumor targeting was studied in a tumor model (melanoma), which is known to express CD105.

2. Materials and methods

2.1. Purification of anti-CD105 mAbs

Rat mAbs directed against mouse CD105 were produced from a hybridoma (clone MJ7/18), which was provided by the Developmental Studies Hybridoma Bank (Iowa University, Iowa City, IA, USA). First, the antibody was purified by protein G-affinity chromatography and dialysis against phosphate buffered saline (PBS, 0.14 M NaCl, 0.006 M Na_2HPO_4, 0.003 M KCl, 0.001 M KH_2PO_4, pH 7.2), followed by a size-exclusion chromatography on a Superdex 200 column (GE Healthcare Life Sciences, Belgium) using a 0.02 M Tris–HCl buffer (pH 7.5) containing 0.15 M NaCl. Then, the purified antibody was concentrated using a membrane filter device with a molecular weight cut-off of 10 kDa (Centrifugal filter units, Merck Millipore, Belgium).

2.2. Direct radioiodination of anti-CD105 mAbs with chloramine-T method

Anti-CD105 mAbs were directly radiolabeled with sodium iodide (Na[^{125}I], 3700 MBq/ml, PerkinElmer Inc., Belgium) using chloramine-T. In brief, a mixture of purified anti-CD105 mAbs (200 μg, 500 μl), Na[^{125}I] (18.5 MBq) and chloramine-T (500 μl, 10 mg/ml) was mixed and reacted for 1 min at room temperature with stirring after 30 s. The reaction was stopped by adding sodium metabisultite (500 μl, 20 mg/ml) as a reducing agent, after which cold sodium iodide (500 μl, 5 mg/ml) was added. The radiolabeled mAbs (^{125}I-anti-CD105 mAbs) were separated from free iodide by passing through a Sephadex G-25 column (GE Healthcare Life Sciences, Belgium), preconditioned with PBS (0.01 M, pH 7.4). All solutions were previously filtrated through a Millipore Millex-GV 0.22 μm filter.

2.3. Indirect radioiodination of D-KRYRR peptide and its conjugation to anti-CD105 mAbs

Anti-CD105 mAbs were indirectly radiolabeled with a peptide prosthetic group (D-KRYRR, JPT Peptide Technologies GmbH, Germany), which was previously radioiodinated. In brief, Na[^{125}I] (37 MBq) was added to D-KRYRR (100 μl, 1 mg/ml PBS 0.01 M pH 7.5). Then, chloramine-T (500 μl, 10 mg/ml) was added to the mixture and reacted for 1 min at room temperature with stirring after 30 s. The reaction was stopped by adding sodium metabisultite (500 μl, 20 mg/ml). The final solution was eluted through a trifunctional reversed-phase cartridge (tC18, 145 mg adsorbent, Waters, Belgium), which was previously rinsed with 1 ml of acetonitrile, 1 ml of water and 500 μl of water containing 0.5% acetonitrile. The radioiodinated peptide was eluted in 400 μl of acetic acid 1 M + 3% potassium chloride in 50% methanol. The solvent was evaporated under a stream of helium prior to reaction with the antibody. The radioiodinated peptide was activated by addition of sulfosuccinimidyl-4-(N-maleimidomethyl)cyclohexane-1-carboxylate (sulfo-SMCC, 50 μl, 10 mg/ml PBS 0.01 M pH 7.5, Thermo Scientific Pierce, Belgium) and borate buffer (0.1 M, 175 μl, pH 8.5), and reacting for 30 min at room temperature. On the other hand, the anti-CD105 mAb (169 μl, 1.8 mg/ml TRIS 0.02 M pH 7.5) was also activated by adding 2-iminothiolane (6 μl, 3 mg/ml PBS 0.01 M pH 7.5, Sigma-Aldrich, Belgium), and incubated for 30 min at room temperature. The thiolated anti-CD105 mAbs were purified using a Sephadex G-25 column. Then, the purified anti-CD105 mAbs were added directly to the vial containing the maleimido-activated radioiodinated KRYRR, and the coupling reaction was performed at room temperature for 45 min, at which point the reaction was quenched by the addition of an excess of iodoacetamide (10 μl, 100 mg/ml PBS 0.01 M pH 7.5, Sigma-Aldrich, Belgium). After 20 min, the mixture was purified over a PD-10 column (GE Healthcare Life Sciences, Belgium) eluted with PBS (0.01 M, pH 7.5) [26].

2.4. Quality controls

Radiochemical yield and purity were performed by using thin layer chromatography (TLC) on ITLC silica gel plates with a mixture of MeOH-H_2O (70:30, *v*/v) as a mobile phase. The TLC migration was followed by radio-TLC detection (Bioscan system 200 imaging scanner). The coupling reaction yield and the purity of indirect radiolabeled mAbs were investigated by TLC on silica gel 60 RP-18 plates with a mixture of acetic acid 1 M + 3% potassium chloride in 50% methanol as a mobile phase. The integrity of the antibody after radiolabeling was checked by sodium dodecyl sulfate-polyacrylamide gel electrophoresis (8% SDS-PAGE gel, under nonreducing conditions). Finally, the detection and the quantification of radioactive bands were performed with a radio-TLC analyzer and a Phosphor Imager (Fujifilm FLA-5100).

2.5. Antibody affinity determination

Saturation binding studies were performed with each of the radioiodinated antibodies (^{125}I-anti-CD105-mAbs and ^{125}I-KRYRR-anti-CD105-mAbs) using B16 cells at a concentration of 2×10^4 cells/ml. Briefly, test solutions were prepared (in duplicate), containing increasing amounts of the radiolabeled antibodies in a total volume of 200 μl of PBS (1% BSA). The solutions were incubated at 4 °C for 2 h, centrifuged for 5 min (5000 rpm), and washed three times with ice-cold PBS (1% BSA). For each concentration of radiolabeled antibodies, nonspecific

binding was determined in the presence of 100-fold excess of unlabeled anti-CD105 antibodies. The data were analyzed with a nonlinear least squares regression method (Graph Pad™ Software Inc., version 5.02) to determine the antibody affinity values (Kd).

2.6. Immunoreactivity determination

The immunoreactive fractions of freshly prepared directly and indirectly radioiodinated antibodies were assessed by the method of Lindmo et al. [36]. Briefly, mouse melanoma cells (B16) were suspended in microfuge tubes at increasing concentrations ranging from 1 to 5 $\times 10^4$ cells in 100 μl PBS (1% BSA). Approximately 21 kBq/0.4 μg and 14 kBq/0.9 μg of respectively ^{125}I-anti-CD105-mAbs and ^{125}I-KRYRR-anti-CD105-mAbs in 100 μl were added to each tube (in duplicate) and stored at 4 °C with stirring every 15 min. Cells were pelleted by centrifugation for 5 min (5000 rpm), washed three times with ice-cold PBS (1% BSA), and subsequently counted for ^{125}I activity. The specific binding was calculated as the ratio of total amount of administered activity to the bound radioactivity and was background corrected. Nonspecific binding of radiolabeled antibodies was less than 5% according to saturation binding studies, and was therefore not used to correct immunoreactivity values [37].

2.7. In vitro stability of ^{125}I-labeled anti-CD105 mAbs in storage solution and in plasma

Chemical stability of purified directly iodinated mAbs (^{125}I-anti-CD105-mAbs) and indirectly iodinated mAbs (^{125}I-KRYRR-anti-CD105-mAbs), stored in a solution of PBS 0.01 M, pH 7.5 was checked for up to one month at 4 °C. Samples were drawn at regular time points and the proportion of free ^{125}I was analyzed by radio-TLC. *In vitro* stability of purified ^{125}I-anti-CD105-mAbs and ^{125}I-KRYRR-anti-CD105-mAbs was also studied in fresh mouse plasma, by incubating the solution of radiolabeled mAbs (1:10 *v*/v dilution at a final concentration of 1.6–2.4 MBq/ml; sodium azide added at 0.02%) at 37 °C with stirring. At different time points (5 min, 15 min, 1 h, 3 h, 6 h, 24 h and 48 h), aliquots of plasma (5 μl) were analyzed using radio-TLC.

2.8. Animal and tumor models

Mouse melanoma cell line (B16F10-luc) was maintained in alpha minimum essential medium (MEM-alpha with glutamine, Gibco-Invitrogen, Belgium) supplemented with 10% heat-inactivated fetal bovine serum (FBS, Gibco-Invitrogen, Belgium), 1% streptomycin–penicillin (Gibco-Invitrogen, Belgium) and 1% MEM non-essential amino acids (Gibco-Invitrogen, Belgium). C57BL/6 J male mice were inoculated subcutaneously in the flanks with 1×10^6 B16F10-luc tumor cells. The mice were used for *in vivo* experiments when the diameter of tumors reached approximately 7–8.5 mm. The biodistribution studies were carried out in compliance with the relevant national laws relating to the conduct of animal experimentation.

2.9. Biodistribution studies using animal-SPECT/CT imaging

SPECT/CT imaging was performed using a preclinical four-headed gamma-camera with integrated CT system (NanoSpect/CT, Bioscan Inc., Washington, D.C., USA) and dedicated multi-pinhole apertures, each with nine pinholes with a diameter of 1.4 mm. These apertures provide a reconstructed resolution of about 1.0 mm in a mouse-sized animal with an average sensitivity of 1800 cps/MBq across the field of view (with ^{99m}Tc). The data were acquired in a step-and-shoot helical mode to include the whole mouse within the field of view. A group of three C57BL/6 J male mice (23–24 g, 5–6 weeks old; Janvier, France) bearing melanoma xenografts was injected intravenously in the lateral tail vein with a freshly prepared solution of ^{125}I-anti-CD105-mAbs (3–3.7 MBq) or ^{125}I-KRYRR-anti-CD105-mAbs (0.6–2.3 MBq). Additionally, to assess the *in vivo* specificity of ^{125}I-KRYRR-anti-CD105-mAbs, a group of three B16 melanoma-bearing mice (blocking group, one or two tumors per mouse) was injected with an excess of unlabeled anti-CD105 mAbs (2 mg mAbs per mouse) 2 h before the injection of the tracer (1.6–1.7 MBq, total of 128 μg mAbs per mouse) as previously described [38]. The blocking group was compared with the group of mice receiving only ^{125}I-KRYRR-anti-CD105-mAbs without a saturating dose. The whole-body SPECT/CT imaging was performed under general anesthesia by inhalation of 1.5% isoflurane (Abbott Laboratories, Belgium) mixed with 21% oxygen gas (2 l/min). The mice were maintained in a prone position on a heated animal bed at 37 °C (Minerve, France). The static SPECT/CT acquisitions were carried out at different time points after injection (1, 3, 6 and 24 h) for mice receiving ^{125}I-anti-CD105-mAbs and (1, 3, 6, 24 and (48 h)) for mice receiving ^{125}I-KRYRR-anti-CD105-mAbs. First, the SPECT images were acquired with a 20% energy window peaked at 28.4 keV, with an acquisition time varying between 20 and 270 s per projection, and with 20 projections. This acquisition time was adapted to compensate for radioiodine clearance in order to ensure significant statistics (>10,000 total counts per projection), and resulted in a total imaging time ranging between 20 and 240 min. The projection data were reconstructed with HiSPECT NG software (Scivis GmbH, Göttingen, Germany) using an iterative reconstruction algorithm with a voxel size of 0.45 mm^3. After SPECT acquisition, the animal remained anesthetized and a CT image was acquired using a standard resolution with a 45 kVp voltage and 500 ms exposure time. The CT projections were reconstructed with a voxel size of $0.15 \times 0.15 \times 0.15$ mm^3 [39].

2.10. SPECT/CT data analyses

After SPECT data reconstruction, the images were analyzed using PMOD software (PMOD™, version 3.4, PMOD Technologies Ltd., Zurich, Switzerland). The regions of interest (ROIs) were delineated on the SPECT/CT fused images. Before the fusion of SPECT and CT images, the SPECT images were normalized. A calibration factor was empirically determined and used to convert the ROI value (total counts) to activity (kBq). A correction was also applied for the acquisition duration and the physical decay during acquisition. The image scale was corrected according to the SPECT calibration factor, the physical decay at the time of injection and the injected dose. This normalization was used to build parametric images of tissue uptake in terms of percentage of the injected dose per milliliter (%ID/ml). 2D ROIs were drawn on consecutive transversal slices that defined a 3D volume of interest around the tissue of interest. The tracer uptake was assessed in the thyroid, tumors, blood and total body. Blood activity over time was quantified by drawing an ROI within the ventricular cavity of heart, based on anatomical CT images fused with SPECT images. A background region was also drawn in the pelvic region. The same background volume was applied for all animal analyses and was representative of tissues with low nonspecific uptake. Tumor uptake was also expressed as a tumor-to-background ratio (T/B), calculated as the mean activity in the tumor region divided by the mean activity obtained in the background region. The tumor uptake of ^{125}I-anti-CD105-mAbs was compared with that obtained for the group of mice receiving ^{125}I-KRYRR-anti-CD105-mAbs, in terms of %ID/ml and T/B ratios. The same comparison was done for the thyroid uptake. Moreover, the clearance of radioactivity over time was compared between the two groups in terms of percentage of the injected dose (%ID), based on the total body quantification. Finally, the tumor uptake of ^{125}I-KRYRR-anti-CD105-mAbs was compared with that obtained for the blocking group, in terms of %ID/ml.

2.11. Statistical analysis

Results are given as means ± SEM values from *n* animals. The data calculations were performed with Prism software (Graph Pad™ Software Inc., version 5.02). The differences in tissue uptake between two

groups were considered significant if the p-values from unpaired t-tests (two-tailed) were ≤0.05 (*), ≤ 0.01 (**) or ≤0.001 (***). The differences in tissue uptake at different times were assessed by the one-way analysis of variance and the Tukey *post-hoc* test.

3. Results

3.1. Anti-CD105 antibody radioiodination and quality controls

For the direct iodination, the radiolabeling of anti-CD105 mAbs with ^{125}I was achieved with a mean radiochemical yield of 90% (n = 5). The radiochemical purity as determined by radio-TLC was higher than 99% (n = 5). The specific activity was 82 ± 1 MBq/mg of mAbs (n = 4). The ^{125}I-to-mAb ratio was about 0.2, which means that approximately one out of five mAb unit carries one ^{125}I atom.

For the indirect iodination, the peptide (D-KRYRR) was radiolabeled with ^{125}I prior to reaction with sulfo-SMCC to maximize peptide concentration during the labeling reaction, and thereby to optimize the radiochemical yield (mean of 96%, n = 4) [26]. The radiochemical purity of ^{125}I-KRYRR after purification with a tC18 cartridge was higher than 95% (n = 4). The coupling of maleimido-derivatized radiolabeled peptide to the thiolated anti-CD105 mAbs was carried out with a mean radiochemical yield of 25% and a specific activity of 25 ± 1 MBq/mg. Before intravenous injection to mice, ^{125}I-KRYRR-anti-CD105-mAbs were concentrated using a membrane filter device, resulting in a purity of 100%.

The gel electrophoresis analysis of purified anti-CD105 mAbs after direct and indirect iodination, under non-reducing conditions, followed by radio-TLC and Phosphor Imager autoradiography revealed that at least 85% of the radioactivity was due to the whole antibody molecule (Fig. 1), and the residual activity was due to protein entities having immunoglobulin origin, as identified by mass spectrometry analyses (electrospray ionization time of flight mass spectrometry) and the NCBInr protein database (data not shown).

The affinity (Kd) of directly and indirectly radioiodinated anti-CD105 mAbs was respectively 0.15 ± 0.05 and 2.37 ± 1.38 μM, as demonstrated by saturation binding curves. The immunoreactivity fractions of ^{125}I-anti-CD105-mAbs and ^{125}I-KRYRR-anti-CD105-mAbs were in the same range and were respectively 84% and 75% (Fig. 2).

3.2. In vitro stability of radioiodinated anti-CD105 mAbs in storage solution and in plasma

In vitro stability of ^{125}I-anti-CD105-mAbs and ^{125}I-KRYRR-anti-CD105-mAbs in storage solution at 4 °C showed a slight deiodination of the antibody, with less than 5% of free iodine up to one month after labeling reaction.

In the plasma, the dissociation was lower than 30% (n = 2–3) up to 48 h after incubation, both for ^{125}I-anti-CD105-mAbs and ^{125}I-KRYRR-anti-CD105-mAbs.

3.3. Comparative biodistribution studies using animal-SPECT/CT imaging

The biodistribution of iodinated anti-CD105 mAbs was imaged in B16-bearing mice, by using SPECT/CT imaging modality, up to 24 h after injection for ^{125}I-anti-CD105-mAbs (n = 3), and up to 48 h after injection for ^{125}I-KRYRR-anti-CD105-mAbs (n = 3). The maximum intensity projection (MIP) images were generated for visual inspection and qualitative analysis of the global kinetics of distribution (Fig. 3). For a more quantitative evaluation, the %ID/ml and the %ID were computed for the tumor, the thyroid, the blood and the total body. From the MIP images of mice receiving ^{125}I-anti-CD105-mAbs, a low tracer uptake in the tumor could be noted, with a weak tumor contrast. Only 2.9 ± 0.2%ID/ml (T/B = 1.2 ± 0.2) was found in the tumor at 6 h after injection, and this value decreased to 0.9 ± 0.3%ID/ml (T/B = 0.9 ± 0.1) after 24 h. In contrast, the tumor uptake of ^{125}I-KRYRR-anti-CD105-mAbs was significantly higher (4.3 ± 0.2%ID/ml, T/B = 4.2 ± 0.3) at 6 h after injection and increased significantly (4.7 ± 0.2%ID/ml, T/B = 5.7 ± 0.1) after 24 h (Fig. 4). The specificity of tumor uptake was investigated by administering a saturating dose of unlabeled anti-CD105 mAbs 2 h before ^{125}I-KRYRR-anti-CD105-mAbs injection. The CD105 binding of ^{125}I-KRYRR-anti-CD105-mAbs was markedly reduced in the tumor at all time points (Fig. 5). The tumor uptake value in the blocking group 24 h after injection (2.6 ± 0.1%ID/ml) was reduced by a factor of 2 compared to mice receiving the tracer only (4.7 ± 0.2%ID/ml).

For the ^{125}I-anti-CD105-mAbs group, the accumulation of iodine in the thyroid started early (2.9 ± 0.1%ID/ml) at 1 h after injection, and increased significantly over time, leading to a very intense hot spot after

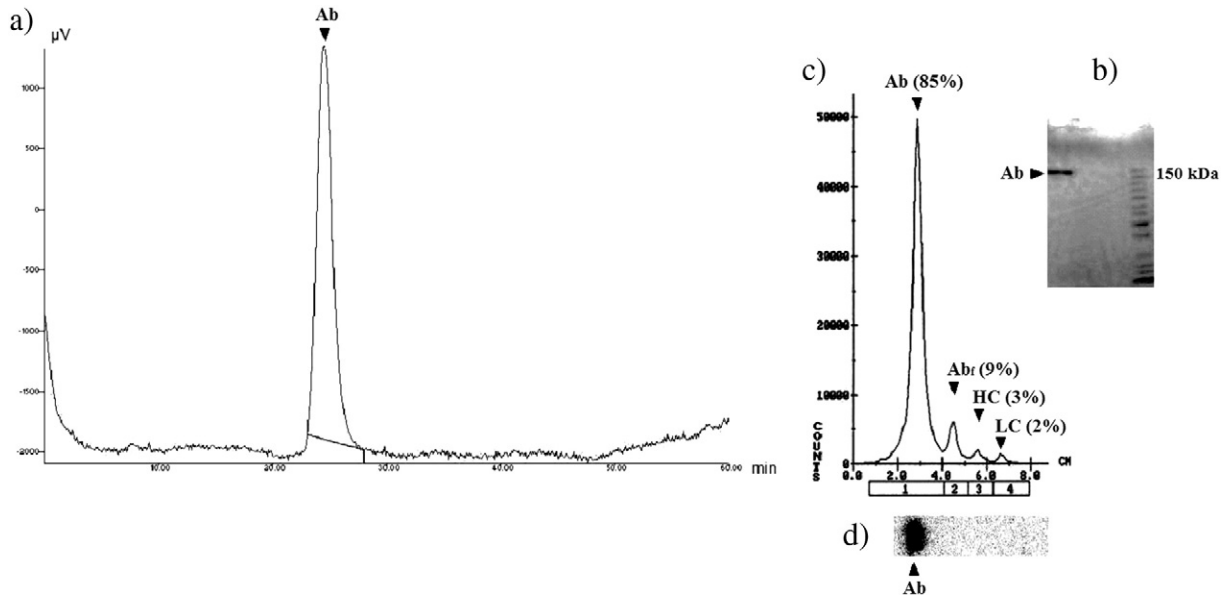

Fig. 1. Chromatographic profile of purified anti-CD105 mAbs using size-exclusion chromatography before antibody radiolabeling [a] and electrophoretic profile of directly iodinated anti-CD105 mAbs using SDS-PAGE 8% under non-reducing conditions [b] followed by radioactivity scanning of the gel through radio-TLC detection [c] and Phosphor Imager analysis [d]. Intact antibody [Ab], antibody fragment [Ab_f], antibody heavy chain [HC] and antibody light chain [LC]. The electrophoretic and Phosphor imaging profiles of indirectly iodinated anti-CD105 mAbs were similar (data not shown).

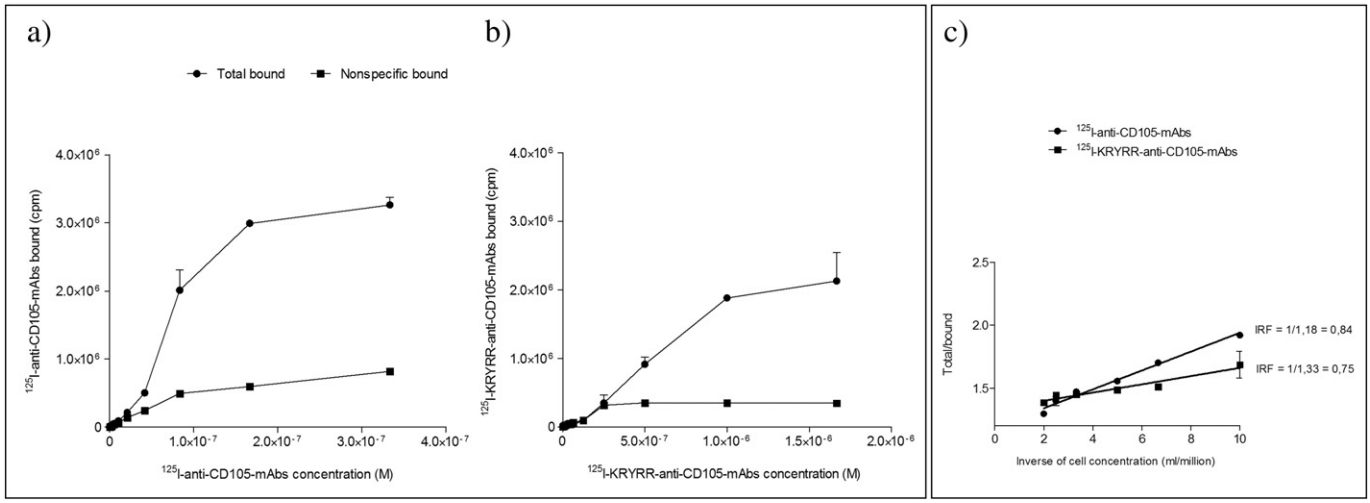

Fig. 2. Saturation binding curves of ^{125}I-anti-CD105-mAbs [a] and ^{125}I-KRYRR-anti-CD105-mAbs [b] to B16 cells. Increasing concentrations of radiolabeled antibodies were incubated with B16 cells at 4 °C for 2 h. Nonspecific binding was determined in the presence of 100-fold excess of unlabeled anti-CD105 antibodies. Bound activity was isolated by centrifuging the cells and washing them three times with ice-cold PBS (1% BSA). Lindmo immunoreactivity testing [c] of ^{125}I-anti-CD105-mAbs (●) and ^{125}I-KRYRR-anti-CD105-mAbs (■): a constant amount of labeled antibodies (21 kBq/0.4 μg and 14 kBq/0.9 μg for respectively ^{125}I-anti-CD105-mAbs and ^{125}I-KRYRR-anti-CD105-mAbs) was added to increasing numbers of B16 cells (10^4 to 5×10^4 cells/ml) and incubated for 2 h at 4 °C. Total/bound data are then plotted as a function of the reciprocal antigen concentration. The immunoreactive fraction (IRF) was determined for conditions representing infinite antigen excess by means of linear extrapolation to the ordinate. Points are means with error bars (n = 2) and the lines were determined by linear regression analysis.

24 h (91.9 ± 4.0%ID/ml) (Fig. 3). In contrast, for the ^{125}I-KRYRR-anti-CD105-mAbs group, the thyroid uptake was significantly lower reaching only 4.4 ± 0.6%ID/ml after 24 h (Fig. 6). A stomach uptake was also observed for the ^{125}I-anti-CD105-mAbs group at 6 h after injection, in parallel with the thyroid uptake, but with no accumulation. A hot spot was observed in the bladder at 3 and 6 h after injection and

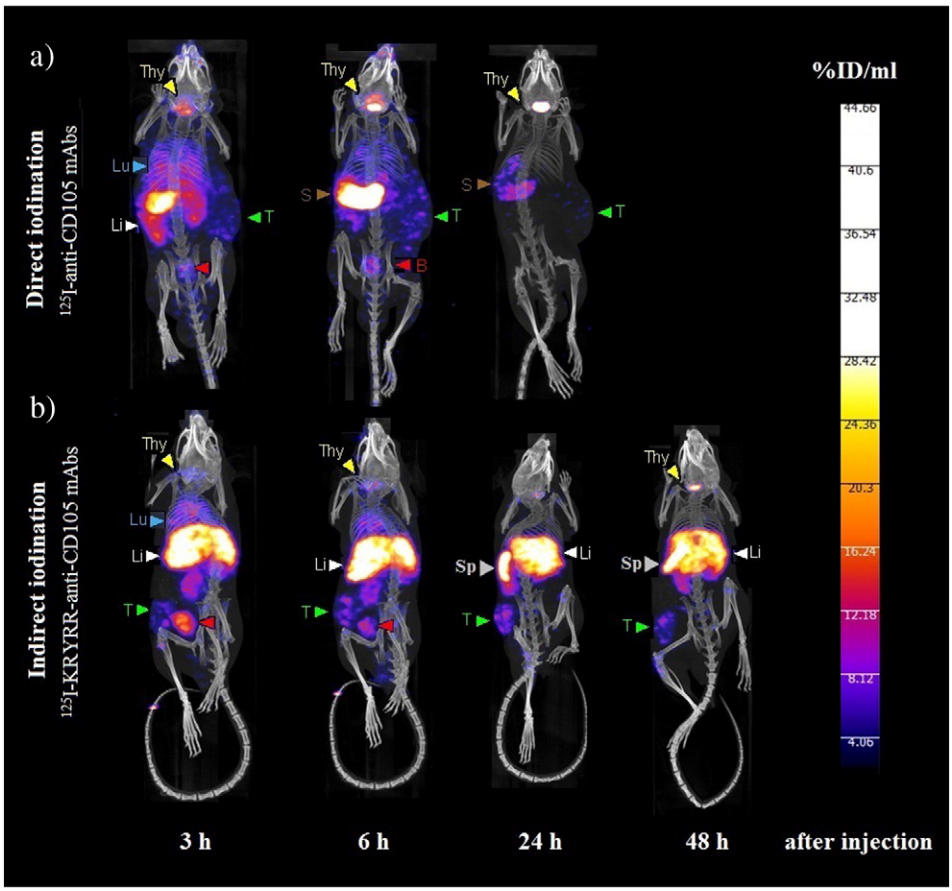

Fig. 3. MIP images from SPECT/CT imaging of two mice bearing B16 tumor, inoculated subcutaneously in the right flank for the mouse receiving ^{125}I-anti-CD105-mAbs (3–3.7 MBq) [a] and in the left flank for the one receiving ^{125}I-KRYRR-anti-CD105-mAbs (0.6–2.3 MBq) [b]. Mice were imaged at 3, 6, 24 (and 48 h) after injection. Color scale, expressed as %ID/ml, indicated the radioactivity uptake levels: in thyroid [Thy], lungs [Lu], liver [Li], stomach [S], spleen [Sp], bladder [B], and in tumors [T].

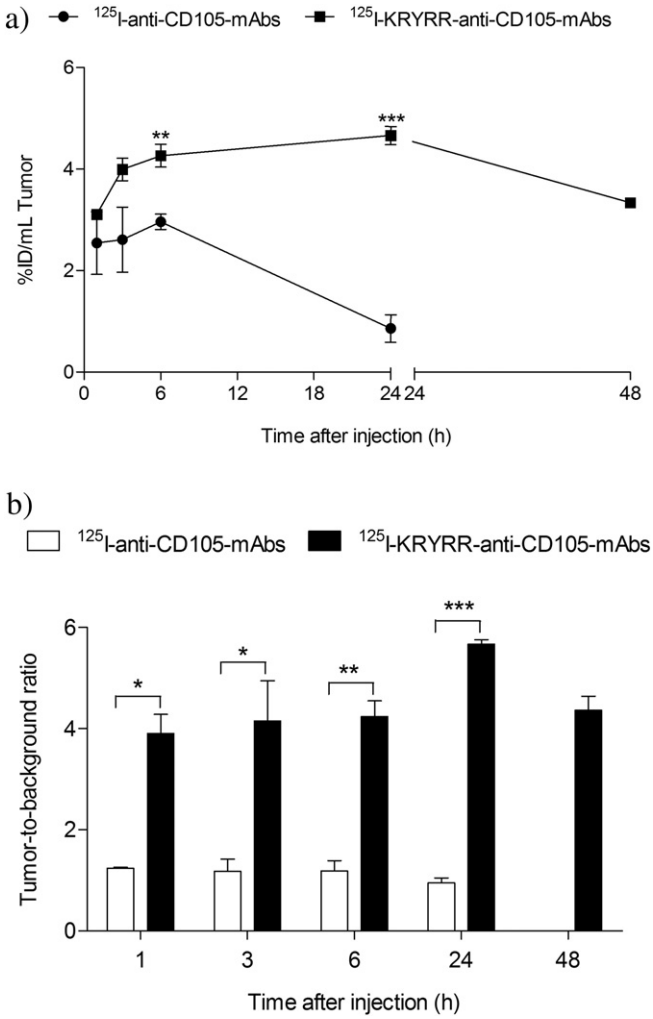

Fig. 4. Tumor uptake expressed as % ID/ml and tumor-to-background ratios (T/B) for B16-bearing C57BL/6 J mice, injected with ^{125}I-anti-CD105-mAbs (3–3.7 MBq per mouse, (●), white bars) [a], or with ^{125}I-KRYRR-anti-CD105-mAbs (0.6–2.3 MBq per mouse, (■), black bars) [b] at 1, 3, 6, 24 (and 48 h) after intravenous injection. Results are expressed as mean ± SEM (n = 3). **p < 0.01 and ***p < 0.001; note the axis break.

was probably related to the urinary excretion of free iodine or products of antibody catabolism (Fig. 3).

Hot spots were also observed in the lungs, the liver and the spleen, which are highly vascularized organs. The lungs showed similar kinetics for the two tracers, with a rapid wash out of the tracers from this non-target tissue. The liver uptake of ^{125}I-anti-CD105-mAbs was transient and was observed particularly at early times after injection (1 and 3 h). In contrast, the radioactivity level in the liver and spleen was

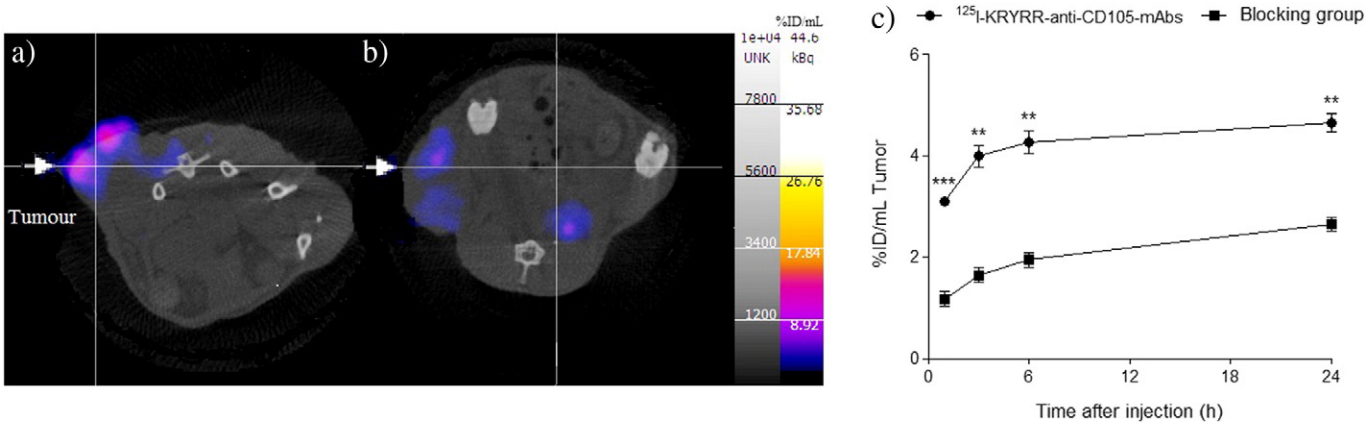

Fig. 5. SPECT/CT images (transaxial sections) of ^{125}I-KRYRR-anti-CD105-mAbs 24 h after injection in B16 melanoma-bearing mice (one tumor per leg) with [a] or without [b] a saturating dose of unlabeled antibodies. White arrows indicate the tumors. [c]: Tumor uptake of ^{125}I-KRYRR-anti-CD105-mAbs (0.6–2.3 MBq, a total of 250 μg mAbs per mouse, (●)) or ^{125}I-KRYRR-anti-CD105-mAbs (1.6–1.7 MBq, a total of 128 μg mAbs per mouse, (■)) after a blocking dose of unlabeled anti-CD105 mAbs (2 mg mAbs per mouse) in B16 melanoma-bearing C57BL/6 J mice at 1, 3, 6 and 24 h after injection. Results are expressed as means ± SEM (n = 3–4). **p < 0.01 and *** p < 0.001.

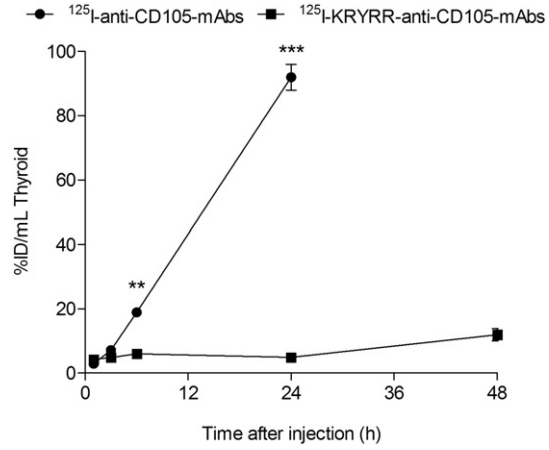

Fig. 6. Thyroid uptake expressed as % ID/ml of ^{125}I-anti-CD105-mAbs (3–3.7 MBq per mouse, (●)) or ^{125}I-KRYRR-anti-CD105-mAbs (0.6–2.3 MBq per mouse, (■)) in B16-bearing C57BL/6 J mice at 1, 3, 6, 24 (and 48 h) after intravenous injection. Results are expressed as mean ± SEM (n = 3). **p < 0.01 and ***p < 0.001.

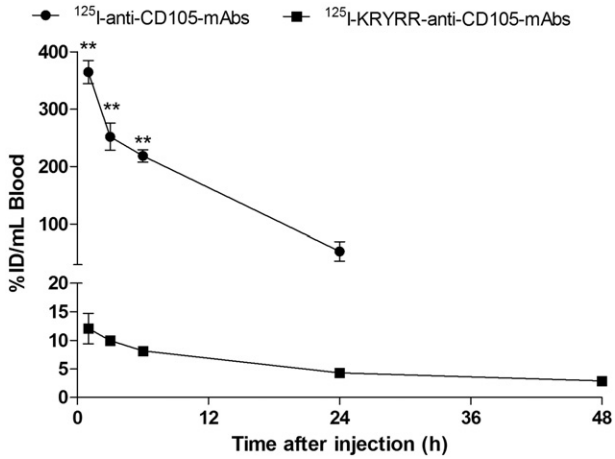

Fig. 8. Blood activity expressed as % ID/ml of ^{125}I-anti-CD105-mAbs (3–3.7 MBq per mouse, (●)) or ^{125}I-KRYRR-anti-CD105-mAbs (0.6–2.3 MBq per mouse, (■)) in B16-bearing C57BL/6 J mice at 1, 3, 6, 24 (and 48 h) after intravenous injection. Results are expressed as mean ± SEM (n = 3). **p < 0.01; note the axis break.

much higher for ^{125}I-KRYRR-anti-CD105-mAbs, and was persistent at late time points (6, 24 and 48 h). The nonspecific tissue uptake by the same organs was also observed in *ex-vivo* studies in C57BL/6 J mice bearing B16 xenografts sacrificed at different time points after injection. In those tissues (thyroid, lungs, spleen, liver and stomach), a comparable biodistribution profile of ^{125}I-labeled anti-CD105 mAbs was observed (data not shown).

Finally, the residual radioactivity in the total body after 24 h was quite low for ^{125}I-anti-CD105-mAbs, suggesting an almost total clearance of the radioactivity. On the contrary, the total clearance of ^{125}I-KRYRR-anti-CD105-mAbs was significantly lower (20.8 ± 2.5%ID) than that of ^{125}I-anti-CD105-mAbs (83.8 ± 3.5%ID) after 24 h (Fig. 7). The tracer concentration in the blood decreased significantly over time for both ^{125}I-KRYRR-anti-CD105-mAbs (12.1 ± 2.6%ID/ml at 1 h to 4.3 ± 0.7%ID/ml at 24 h) and ^{125}I-anti-CD105-mAbs (364.7 ± 20.0%ID/ml at 1 h to 53.0 ± 17.0%ID/ml at 24 h) (Fig. 8). The blood activity was significantly higher for ^{125}I-anti-CD105-mAbs at early times after injection (1, 3 and 6 h).

4. Discussion

To date, the only antiangiogenic antibody approved for clinical indications is bevacizumab [40,41]. There is a need to develop more antibodies against targets highly expressed on tumor endothelium. In this context, CD105 may be an attractive target for radioimmunotherapy, as previous studies explored the imaging and therapeutic potential of anti-CD105 mAbs through conventional radioiodination methods [3,19]. However, these studies did not investigate the *in vivo* stability of iodinated mAbs. Our study compared the biodistribution of directly and indirectly iodinated anti-CD105 mAbs. Overall, our results highlight even more clearly that the radioiodination procedure had a major impact on the pharmacokinetics of labeled anti-CD105 mAbs, with important consequences in terms of tumor uptake.

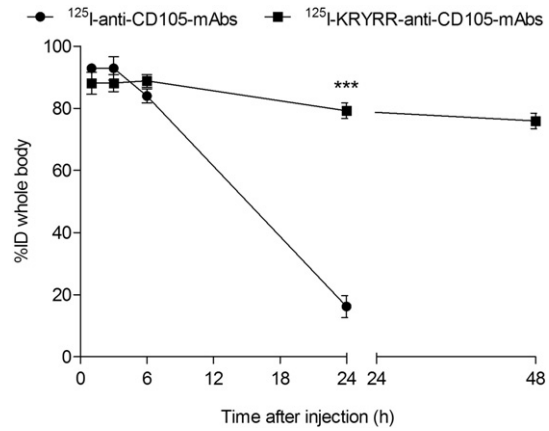

Fig. 7. Total body clearance expressed as %ID of ^{125}I-anti-CD105-mAbs (3–3.7 MBq per mouse, (●)) or ^{125}I-KRYRR-anti-CD105-mAbs (0.6–2.3 MBq per mouse, (■)) in B16-bearing C57BL/6 J mice at 1, 3, 6, 24 (and 48 h) after intravenous injection. Results are expressed as mean ± SEM (n = 3). ***p < 0.001; note the axis break.

The direct iodination of anti-CD105 mAbs led to a rapid *in vivo* dehalogenation, as reflected by high radioiodine levels in the thyroid and stomach [42,43]. Since we observed a good *in vitro* chemical stability of radioiodinated mAbs, the results suggest that *in vivo* catabolism is responsible for the important antibody dehalogenation [44]. The iodine uptake in these organs is mediated by the sodium iodide (Na^+/I^-) symporter (NIS), an integral membrane protein which is expressed in thyroid epithelial cells and in stomach tissue [45]. The radioactivity accumulation in the thyroid can be considered as the result of *in vivo* deiodination (Fig. 6). As the stomach is not known to utilize the iodine in any biological process, the iodine freely exits through diffusion and does not result in prolonged exposure as in the thyroid [46]. The released iodine was rapidly cleared from the body, and may explain the low tumor uptake and contrast (Fig. 7). In contrast, the injection of indirectly iodinated anti-CD105 mAbs to mice led to a significantly decreased dehalogenation process since the thyroid uptake was 20 orders of magnitude lower, 24 h after injection (Fig. 6).

The slower body clearance of ^{125}I-KRYRR-anti-CD105-mAbs compared to that of ^{125}I-anti-CD105-mAbs led to a higher tissue accumulation of the tracer, especially in tumors, and an improved tumor contrast over time due to a highly specific uptake (Fig. 7). This pharmacokinetic profile will most probably cause an increased radiation dose. The higher blood activity of ^{125}I-anti-CD105-mAbs at early times after injection is due to the rapid and higher *in vivo* deiodination (Fig. 8). The blood activity decreased over time for the two tracers in accordance with the pattern of the whole body clearance. Finally, the slow pharmacokinetics of ^{125}I-KRYRR-anti-CD105-mAbs are in accordance with what is known for whole antibodies. Indeed, it is well known that antibody-based radiotracers require extended *in vivo* circulation times for optimal tumor targeting, typically 2–4 days.

The rationale for using D-KRYRR was based on previous studies, which showed the retention improvement of radioiodine in tumor cells [26]. This peptide contains three arginine residues (R) adding positive charges. The arginine side chain is indeed the most basic (pKa = 13.2) of the naturally occurring amino acids. Because some mAbs,

such as anti-CD105 mAbs, are internalized and directed to the lysosomes after binding to cell surface receptors, there is a risk of subsequent degradation of mAbs inside the tumor cells and the release of free iodine [19,47]. Similarly to the positively charged molecules that are often used as lysosomal markers [48], the positively charged catabolites generated during mAb proteolysis are highly retained by lysosomes, resulting in prolonged enhancement of tumor cell retention [26]. Moreover, the peptide bound in D-KRYRR would be relatively resistant to the action of proteases in the lysosomes. Indeed, the endogenous lysosomal proteases readily degrade endocytosed proteins composed of L-amino acids but not proteins composed of D-amino acids, which are trapped in lysosomes [49,50]. For all these reasons, a much more favorable kinetic pattern was achieved with ^{125}I-KRYRR-anti-CD105-mAbs, so that the percentage of activity retained in tumors was nearly 5.5 times higher after 24 h compared to ^{125}I-anti-CD105-mAbs. These results are better than that of obtained with ^{125}I-KRYRR-anti-EGFR mAbs in U87 MGΔEGFR xenografts, since the tumor retention was increased by a factor of approximately 3 at 24 h compared with directly iodinated anti-EGFR mAbs [26]. Finally, there was also an improvement of the tumor contrast over time, which is much more favorable for imaging purposes.

The maintained specificity of indirectly iodinated anti-CD105 mAbs was confirmed by *in vitro* and *in vivo* saturation experiments, suggesting the selective accumulation of ^{125}I-KRYRR-anti-CD105-mAbs in the tumors and the preservation of the CD105 recognition property by the antibody after radiolabeling. In fact, the administration of unlabeled mAbs in excess before the tracer injection induced the saturation of the CD105 binding sites and significantly decreased the CD105 binding of the tracer in tumors (Fig. 5). These results confirmed the antigen-specific binding and the preservation of antibody immunoreactivity.

As expected, a reticuloendothelial system uptake was observed according to the known catabolism of mAbs, liver and spleen being the preferential sites for the nonspecific uptake [51,52]. The liver uptake of ^{125}I-anti-CD105-mAbs was transient, reflecting *in vivo* deiodination and the release of iodine outside the cells after catabolism. In contrast, the liver and spleen uptakes of ^{125}I-KRYRR-anti-CD105-mAbs were persistent, reflecting the cell retention of the tracer. The same profile in nonspecific tissue uptake was observed with ^{125}I-KRYRR-anti-EGFR mAbs compared to ^{125}I-anti-EGFR mAbs. For the indirectly iodinated anti-EGFR mAbs, the liver and spleen levels were significantly higher than those for directly iodinated anti-EGFR mAbs, whereas thyroid, blood and stomach levels were significantly lower [26]. Finally, the lung uptake may be explained by the constitutive expression of CD105 in normal blood vessels, especially in vascularized tissues. In fact, previous studies have shown that high levels of CD105 expression are seen in the distal vessels of mouse lung [53].

The radiometalated mAbs constitute another class of residualizing labels, such as the radionuclide from indium-, yttrium- and zirconium-labeled mAbs. They are residualized in the lysosomes after lysosomal processing in the form of lysine adducts of the respective metal chelates, resulting in enhanced retention of the nuclide in the tumor, reduced residence time in the blood, and consequently tumor-to-non-tumor discrimination [24,54,55]. It has been suggested that the final metallic catabolites are also residualizing labels for the same reasons as those of iodinated catabolites. They are trapped and impermeable to membrane because they cannot be digested by lysosomal hydrolases [24]. In a previous study, we described the biodistribution profile of ^{89}Zr-anti-CD105-mAbs before and after gold nanoparticle conjugation by using non-invasive positron emission tomography (PET) in C57BL/6 J mice bearing melanoma xenograft [56]. The kinetic profile of unconjugated ^{89}Zr-anti-CD105-mAbs was comparable to that of ^{125}I-KRYRR-anti-CD105-mAbs. The PET/CT images showed the same pattern of nonspecific uptake in liver, spleen and lungs. The tumor uptake of ^{89}Zr-anti-CD105-mAbs reached a peak after 24 h (6.5 ± 0.5%ID/ml) and was maintained high at late times (5.8 ± 0.6%ID/ml until to 48 h). The tumor contrast of ^{89}Zr-anti-CD105-mAbs (T/B = 5.4 ± 0.3) was in the same range as that of ^{125}I-KRYRR-anti-CD105-mAbs (T/B = 5.7 ± 0.1) after 24 h.

Finally, it is of interest that other types of residualizing radioiodine labels [24,30–35,57–59] could be tested with anti-CD105 mAbs, such as N^{ε}-(3-[^{125}I]iodobenzoyl)-Lys^{5}-N^{α}-maleimido-Gly^{1}-GEEEK. This new prosthetic group, consisting of three D-glutamates, a D-lysine carrying an [^{125}I]iodobenzoyl moiety, and a maleimide function was conjugated to an internalizing anti-EGFR mAb and showed a high improvement of radioactivity internalization into cells *in vitro* (15-fold) by comparison with the direct radioiodination, and an increase of the tumor uptake *in vivo* (3-fold higher) [60].

5. Conclusions

A major challenge in cancer immunodetection, imaging and therapy is to maximize the amount of antibody localizing at the tumor site, while avoiding an excessive accumulation in normal organs. We here focused on iodinated antibodies directed against CD105, an interesting cancer target. We found that the radiolabeling procedure had a major impact on the *in vivo* stability and the tumor uptake. The directly iodinated antibodies were unstable *in vivo*, with a rapid accumulation in the thyroid, a fast clearance from the body, and an absence of tumor accumulation. In contrast, the indirectly iodinated anti-CD105 mAbs, using D-KRYRR peptide, led to more stable tracers, prevented the *in vivo* deiodination, and increased the radiotracer retention in the tumor. The latter compound deserves further investigation for imaging and eventual therapeutic purposes.

Conflict of interest statement

The authors declare that they have no conflict of interest.

Acknowledgments

This work was supported by grants from the Region Walloon through the "THERAPLUS" project and the Belgian National Fund for Scientific Research (FNRS-TELEVIE). The hybridoma (clone MJ7/18) was obtained from the Developmental Studies Hybridoma Bank developed under the auspices of the NICHD and maintained by The University of Iowa, Department of Biology, Iowa City, IA 52242.

References

[1] Bernabeu C, Conley BA, Vary CP. Novel biochemical pathways of endoglin in vascular cell physiology. J Cell Biochem 2007;102:1375–88.
[2] Wikström P, Lissbrant IF, Stattin P, Egevad L, Bergh A. Endoglin (CD105) is expressed on immature blood vessels and is a marker for survival in prostate cancer. Prostate 2002;51:268–75.
[3] Fonsatti E, Jekunen AP, Kairemo KJ, Coral S, Snellman M, Nicotra MR, et al. Endoglin is a suitable target for efficient imaging of solid tumors: *in vivo* evidence in a canine mammary carcinoma model. Clin Cancer Res 2000;6:2037–43.
[4] Bernabeu C, Lopez-Novoa JM, Quintanilla M. The emerging role of TGF-beta superfamily coreceptors in cancer. Biochim Biophys Acta 1792;2009:954–73.
[5] El-Gohary YM, Silverman JF, Olson PR, Liu YL, Cohen JK, Miller R, et al. Endoglin (CD105) and vascular endothelial growth factor as prognostic markers in prostatic adenocarcinoma. Am J Clin Pathol 2007;27:572–9.
[6] Beresford MJ, Harris AL, Ah-See M, Daley F, Padhani AR, Makris A. The relationship of the neo-angiogenic marker, endoglin, with response to neoadjuvant chemotherapy in breast cancer. Br J Cancer 2006;95:1683–8.
[7] Brewer CA, Setterdahl JJ, Li MJ, Johnston JM, Mann JL, McAsey ME. Endoglin expression as a measure of microvessel density in cervical cancer. Obstet Gynecol 2000;96:224–8.
[8] Sun T, Sun BC, Ni CS, Zhao XL, Wang XH, Qie S, et al. Pilot study on the interaction between B16 melanoma cell-line and bone-marrow derived mesenchymal stem cells. Cancer Lett 2008;263:35–43.
[9] Hussein MR. Transforming growth factor-beta and malignant melanoma: molecular mechanisms. J Cutan Pathol 2005;32:389–95.
[10] Letamendía A, Lastres P, Almendro N, Raab U, Bühring HJ, Kumar S, et al. Endoglin, a component of the TGF-beta receptor system, is a differentiation marker of human choriocarcinoma cells. Int J Cancer 1998;76:541–6.
[11] Charpin C, Dales JP, Garcia S, Carpentier S, Djemli A, Andrac L, et al. Tumor neoangiogenesis by CD31 and CD105 expression evaluation in breast carcinoma tissue microarrays. Clin Cancer Res 2004;10:5815–9.

[12] Li C, Gardy R, Seon BK, Duff SE, Abdalla S, Renehan A, et al. Both high intratumoral microvessel density determined using CD105 antibody and elevated plasma levels of CD105 in colorectal cancer patients correlate with poor prognosis. Br J Cancer 2003;88:1424–31.
[13] Kumar S, Ghellal A, Li C, Byrne G, Haboubi N, Wang JM, et al. Breast carcinoma: vascular density determined using CD105 antibody correlates with tumor prognosis. Cancer Res 1999;59:856–61.
[14] Romani AA, Borghetti AF, Del Rio P, Sianesi M, Soliani P. The risk of developing metastatic disease in colorectal cancer is related to CD105-positive vessel count. J Surg Oncol 2006;93:446–55.
[15] Marioni G, D'Alessandro E, Giacomelli L, Staffieri A. CD105 is a marker of tumour vasculature and a potential target for the treatment of head and neck squamous cell carcinoma. J Oral Pathol Med 2010;39:361–7.
[16] Rosen LS, Hurwitz HI, Wong MK, Goldman J, Mendelson DS, Figg WD, et al. A phase I first-in-human study of TRC105 (anti-endoglin antibody) in patients with advanced cancer. Clin Cancer Res 2012;18:4820–9.
[17] Olafsen T, Kenanova VE, Wu AM. Imaging tumor xenografts using radiolabeled antibodies. In: Kontermann R, Dübel S, editors. Antibody engineering. Springer-Verlag: Berlin Heidelberg; 2010. p. 491–506.
[18] Verel I, Visser GW, Vosjan MJ, Finn R, Boellaard R, van Dongen GA. High-quality ^{124}I-labelled monoclonal antibodies for use as PET scouting agents prior to ^{131}I-radioimmunotherapy. Eur J Nucl Med Mol Imaging 2004;31:1645–52.
[19] Tabata M, Kondo M, Haruta Y, Seon BK. Antiangiogenic radioimmunotherapy of human solid tumors in SCID mice using ^{125}I-labeled anti-endoglin monoclonal antibodies. Int J Cancer 1999;82:737–42.
[20] Geissler F, Anderson SK, Venkatesan P, Press O. Intracellular catabolism of radiolabeled anti-μ antibodies by malignant B-cells. Cancer Res 1992;52:2907–15.
[21] Meredith RF, LoBuglio AF, Plott WE, Orr RA, Brezovich IA, Russell CD, et al. Pharmacokinetics, immune response, and biodistribution of iodine-131-labeled chimeric mouse/human IgG1,k 17-1 A monoclonal antibody. J Nucl Med 1991;32:1162–8.
[22] Fan Z, Tang Z, Liu K, Zhou D, et al. Radioiodinated anti-hepatocellular carcinoma (HCC) ferritin. targeting therapy, tumor imaging and anti-antibody response in HCC patients with hepatic arterial infusion. J Cancer Res Clin Oncol 1992;118:371–6.
[23] Miraldi F. Monoclonal antibodies and neuroblastoma. Semin Nucl Med 1989;19:282–94.
[24] Govindan SV, Mattes MJ, Stein R, McBride BJ, Karacay H, Goldenberg DM, et al. Labelling of monoclonal antibodies with diethylenetriaminepentaacetic acid-appended radioiodinated peptides containing D-amino acids. Bioconjug Chem 1999;10:231–40.
[25] Mattes MJ, Griffiths GL, Diril H, Goldenberg DM, Ong GL, Shih LB, et al. Processing of antibody-radioisotope conjugates after binding to the surface of tumor cells. Cancer 1994;73:787–93.
[26] Foulon CF, Reist CJ, Bigner DD, Zalutsky MR. Radioiodination via d-amino acid peptide enhances cellular retention and tumor xenograft targeting of an internalizing anti-epidermal growth factor receptor variant III monoclonal antibody. Cancer Res 2000;60:4453–60.
[27] Geissler F, Anderson SK, Press O. Intracellular catabolism of radiolabeled anti-CD3 antibodies by leukemic T cells. Cell Immunol 1991;137:96–110.
[28] Press OW, Farr AG, Borroz KI, Anderson SK, Martin PJ. Endocytosis and degradation of monoclonal antibodies targeting human B-cell malignancies. Cancer Res 1989;49:4906–12.
[29] Shih LB, Thorpe SR, Griffiths GL, Diril H, Ong GL, Hansen HJ, et al. The processing and fate of antibodies and their radiolabels bound to the surface of tumor cells *in vitro*: A comparison of nine antibodies. J Nucl Med 1994;35:899–908.
[30] Stein R, Goldenberg DM, Thorpe SR, Basu A, Mattes MJ. Effects of radiolabeling monoclonal antibodies with a residualizing iodine radiolabel on the accreation of radioisotope in tumors. Cancer Res 1995;55:3132–9.
[31] Reist CJ, Garg PK, Alston KL, Bigner DD, Zalutsky MR. Radioiodination of internalizing monoclonal antibodies using N-succinimidyl 5-iodo-3-pyridine-carboxylate: *in vitro* studies. Cancer Res 1996;56:4970–7.
[32] Ali SA, Warren SD, Richter KY, Badger CC, Eary JF, Press OW, et al. Improving the tumor retention of radioiodinated antibody: aryl carbohydrate adducts. Cancer Res 1990;50:783s–8s.
[33] Zalutsky MR, Garg PK, Narula AS. Labeling monoclonal antibodies with halogen nuclides. Acta Radiol Suppl 1990;374:141–5.
[34] Srivastava PC, Buchsbaum DJ, Allred JF, Brubaker PG, Hanna DE, Spicker JK. A new conjugating agent for radioiodination of proteins: low *in vivo* deiodination of a radiolabeled antibody in a tumor model. Biotechniques 1990;8:536–45.
[35] Li J, Shi L, Wang C, Zhang X, Jia L, Li X, et al. Preliminary biological evaluation of ^{125}I-labeled anti-carbonic anhydrase IX monoclonal antibody in the mice bearing HT-29 tumors. Nucl Med Commun 2011;32:1190–3.
[36] Lindmo T, Boven E, Cuttitta F, Fedorko J, Bunn Jr PA. Determination of the immunoreactive fraction of radiolabeled monoclonal antibodies by linear extrapolation to binding at infinite antigen excess. J Immunol Methods 1984;72:77–89.
[37] Haisma HJ, Pinedo HM, Silva CA, Boven E. Determination of the immunoreactive fraction of radiolabeled monoclonal antibodies directed against intracellular antigens. J Immunol Methods 1992;154:55–60.
[38] Hong H, Yang Y, Zhang Y, et al. Positron emission tomography imaging of CD105 expression during tumor angiogenesis. Eur J Nucl Med Mol Imaging 2011;38:1335–43.
[39] Forrer F, Valkema R, Bernard B, Schramm NU, Hoppin JW, Rolleman E, et al. *In vivo* radionuclide uptake quantification using a multi-pinhole SPECT system to predict renal function in small animals. Eur J Nucl Med Mol Imaging 2006;33:1214–7.
[40] Nassiri F, Cusimano MD, Scheithauer BW, Rotondo F, Fazio A, Yousef GM, et al. Endoglin (CD105): a review of its role in angiogenesis and tumor diagnosis, progression and therapy. Anticancer Res 2011;31:2283–90.
[41] Cohen MH, Gootenberg J, Keegan P, Pazdur R. FDA drug approval summary: bevacizumab (Avastin) plus carboplatin and paclitaxel as first-line treatment of advanced/metastatic recurrent nonsquamous non-small cell lung cancer. Oncologist 2007;12:713–8.
[42] Bakker WH, Krenning EP, Breeman WA, Kooij PP, Reubi JC, Koper JW, et al. *In vivo* use of a radioiodinated somatostatin analogue: dynamics, metabolism, and binding to somatostatin receptor-positive tumors in man. J Nucl Med 1991;32:1184–9.
[43] Garg PK, Alston KL, Welsh PC, Zalutsky MR. Enhanced binding and inertness to dehalogenation of α-melanotropic peptides labelled using N-succinimidyl-3-iodobenzoate. Bioconjug Chem 1996;7:233–9.
[44] Ram S, Buchsbaum DJ. Radioiodination of monoclonal antibodies D612 and 17-1 A with 3-iodophenylisothiocyanate and their biodistribution in tumor-bearing nude mice. Cancer 1994;73:808–15.
[45] Filetti S, Bidart JM, Arturi F, Caillou B, Russo D, Schlumberger M. Sodium/iodide symporter: a key transport system in thyroid cancer cell metabolism. Eur J Endocrinol 1999;141:443–57.
[46] Carrasco N. Iodide transport in the thyroid gland. Biochim Biophys Acta 1993;1154:65–82.
[47] Reist CJ, Archer GE, Kurpad SN, Wikstrand CJ, Vaidyanathan G, Willingham MC, et al. Tumor-specific anti-epiderma growth factor receptor variant III monoclonal antibodies: use of the tyramine-cellobiose radioiodination method enhances cellular retention and uptake in tumor xenografts. Cancer Res 1995;55:4375–82.
[48] Holtzman E. Lysosomes. New York: Plenum Press; 1989 95–100.
[49] Milton RC, Milton SC, Kent SB. Total chemical synthesis of a D-enzyme: the enantiomers of HIV-1 protease show demonstration of reciprocal chiral substrate specificity. Science 1992;256:1445–8.
[50] Ehrenreich BA, Cohn ZA. The fate of peptides pinocytosed by macrophages *in vitro*. J Exp Med 1969;129:227–43.
[51] van den Abbeele AD, Aaronson RA, Taube RA, Adelstein SJ, Kassis AI. Preadsorption of radiolabeled monoclonal antibodies to liver and spleen tissues leads to higher tumor-to-normal-tissue ratios. J Nucl Med Allied Sci 1990;34:94–102.
[52] Sands H, Jones PL. Methods for the study of the metabolism of radiolabeled monoclonal antibodies by liver and tumor. J Nucl Med 1987;28:390–8.
[53] Mahmoud M, Borthwick GM, Hislop AA, Arthur HM. Endoglin and activin receptor-like-kinase 1 are co-expressed in the distal vessels of the lung: implications for two familial vascular dysplasias, HHT and PAH. Lab Investig 2009;89:15–25.
[54] Franano FN, Edwards WB, Welch MJ, Duncan JR. Metabolism of receptor targeted ^{111}In-DTPA-glycoproteins: identification of ^{111}In-DTPA-ε-lysine as the primary metabolic and excretory product. Nucl Med Biol 1994;8:1023–34.
[55] Vugts DJ, van Dongen GA. ^{89}Zr-labeled compounds for PET imaging guided personalized therapy. Drug Discov Today Technol 2011;8:e53–61.
[56] Karmani L, Bouchat V, Bouzin C, Levêque P, Labar D, Bol A, et al. ^{89}Zr-labelled anti-endoglin antibody-targeted gold nanoparticles for imaging cancer: implications for future cancer therapy. Nanomedicine (UK) 2014;9:1923–37.
[57] Ram S, Buchsbaum DJ. Radioiodination of monoclonal antibodies D612 and 17-1 A with 3-iodophenylisothiocyanate and their biodistribution in tumor-bearing nude mice. Cancer 1994;73:808–15.
[58] Zalutsky MR, Narula AS. A method for the radiohalogenation of proteins resulting in decreased thyroid uptake of radioiodine. Int J Rad Appl Instrum A 1987;38:1051–5.
[59] Wilbur DS, Hadley SW, Hylarides MD, Abrams PG, Beaumier PA, Morgan AC, et al. Development of a stable radioiodinating reagent to label monoclonal antibodies for radiotherapy of cancer. J Nucl Med 1989;30:216–26.
[60] Vaidyanathan G, Alston KL, Bigner DD, Zalutsky MR. Nepsilon-(3-[*I]iodobenzoyl)-Lys5-Nalpha-maleimido-Gly1-GEEEK ([*I]IB-Mal-D-GEEEK): a radioiodinated prosthetic group containing negatively charged D-glutamates for labeling internalizing monoclonal antibodies. Bioconjug Chem 2006;17:1085–92.